

Fixed Point Iterative Schemes for Initial Shape Identification

M. Sellier

The question of interest in the present study is "given a work-piece subject to prescribed loads, how to define its initial shape such that the work-piece matches a prescribed geometry after deformation?". This question is particularly relevant in forming processes where the tolerated mismatch between the deformed and desired geometries may be lower than a Micron. To tackle this optimal shape design problem, a range of fixed point iterative schemes is proposed, i.e. the next initial shape is deduced from the previous one by subtracting the error in the previous final shape possibly corrected by an additional term. The required form of this additional, corrective term is revealed through a convergence analysis of the schemes. The schemes are applied to a test problem and their performance compared. The problem consists in designing the hole in a membrane such that its contour matches a prescribed shape when the membrane is stretched by a given load.

1 Introduction

A question engineers often have to face is, "given a set of loads applied to a solid body, what should be the initial geometry so that the end geometry (after deformation) matches the prescribed one?". The development of efficient and accurate numerical techniques such as the finite element method and the well-established theory of optimal shape design (Pironneau (1984); Sokolowski and Zolesio (1992)) allowed significant progress towards the solution to such inverse problems. A popular approach consists in parameterizing somehow the contour of the work-piece, defining an objective function related to the mismatch between the deformed and desired work-piece geometries and applying the extensive theory of optimization in order to find the values of the parameters which minimize the objective function. This approach has proven its applicability for the problem of pre-form or tool design in the metal forging process (see Vieilledent and Fourment (2001); Sousa et al. (2002); Chung et al. (2003) and references therein). Many authors favour gradient-based optimization techniques and the condition for the success of these is the accurate and efficient evaluation of the sensitivities, i.e. the derivative of the objective function with respect to the parameters. The sensitivity analysis may be performed using the finite difference method, the direct differentiation method (Vieilledent and Fourment (2001); Sousa et al. (2002)) or the adjoint-state method (Chung et al. (2003); Sprekels et al. (1996)). In many practical cases, the pragmatic user of a commercial code for the computation of the deformations is bounded to the use of the finite difference method to compute the sensitivities, and this approach is known for its lack of accuracy and efficiency (Chung et al. (2003)).

Another method introduced by Park et al. (1983) consists in starting from the desired work-piece geometry and performing the deformation simulation in reverse. This concept was exploited with success by many authors (see Zhao et al. (1995) and references therein). Despite its success, the implementation of this method in commercial codes is difficult in practice making it out of reach of the widest engineering community.

The fixed point iterative method described in the present work offers an alternative which avoids the difficulty of computing the sensitivities and is fully compatible with the usage of commercial codes. The idea is to "test and correct". More precisely, the difference between the deformed and desired geometries at a given iteration gives the input on how to correct the previous guess to the initial shape. How to define the difference between the deformed and desired geometries and how to reflect this difference on the previous guess to the initial shape are important and non-trivial questions which affect the success and the efficiency of the scheme. Such a method is used in Jernberg (2003), for example, to find very efficiently the optimal tool geometry to compensate for the spring back effect. A simple criterion based on the closest distance from the deformed to the desired geometry is used to correct the previous guess to the design. Other more sophisticated correcting stages were recently derived by Shim and co-workers in the context of the optimal blank shape design. These include the sensitivity method (Shim and Son (2001)), the initial velocity of boundary nodes (INOV) method (Son and Shim (2003)) and the radius vector of boundary nodes method (Shim (2004)).

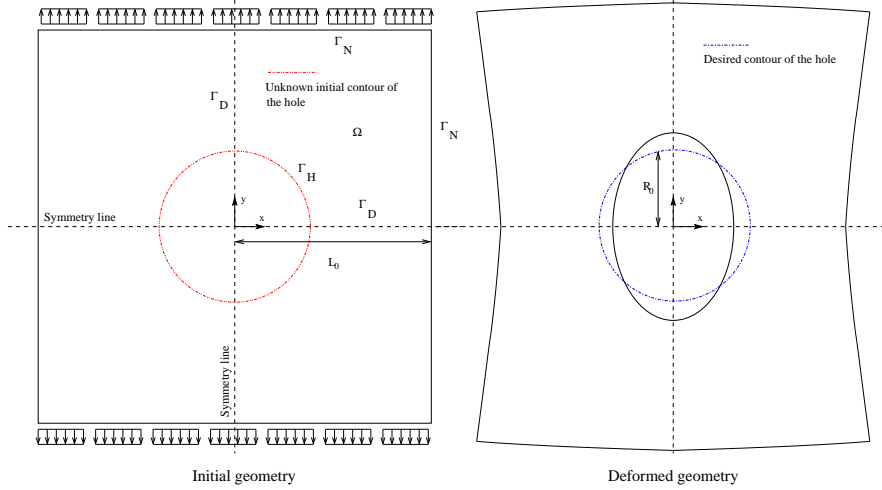


Figure 1: Sketch of the general forward problem.

A similar concept, based on a fixed point iterative scheme to update the location of a set of boundary points, was exploited in Sellier (2005) to identify the required initial geometry in the context of high-precision glass forming. This method proved its applicability and its efficiency, and was easily implemented in a commercial code. In spite of the non-linear viscoelastic behaviour of the glass, only few iterations were required to reduce the mismatch between the deformed and desired work-piece geometries below one Micron. A formal analysis explained the good convergence property of the iterative scheme and revealed that the convergence can only be guaranteed when the deformations are dominated by shear or volumetric strains.

The aim of the present work is to present a modified scheme which circumvents theoretically this restriction. The main idea remains essentially the same but a corrective term is added for the update of the boundary points locations. The next two sections are devoted to the description of the geometric shape optimization problem under consideration and the fixed point iterative scheme. An analysis of the convergence of the scheme follows and the required form of the corrective term is derived. The performance of the schemes is then compared and conclusions are drawn.

2 Description of the Forward Problem

As illustrated on Figure 1, a linear elastic membrane perforated by a hole of contour Γ_H is stretched by a prescribed set of load. The membrane is a $2L_0 \times 2L_0$ square, and the contour of the perforated hole is sought so that it matches a circle of radius R_0 when the membrane is deformed. The geometry shown on Figure 1 corresponds precisely to the one presented by Alberty and co-workers (Alberty et al. (2002)) and the solution to the forward problem is obtained using the Matlab implementation for P_1 and Q_1 finite element provided by the authors. Only a short overview of the theoretical background is reported here for completeness, and further details can be found in Alberty et al. (2002). The problem considered is a plane stress one and the two components of the displacement vector $\mathbf{U} = (U_x, U_y) \in H^1(\Omega)$, subject to Neumann boundary conditions on $\Gamma_N \cup \Gamma_H$ and Dirichlet boundary conditions on Γ_D , must satisfy the following Navier-Lamé equations,

$$(\lambda + \mu)(\nabla \operatorname{div} \mathbf{U}) + \mu \Delta \mathbf{U} = 0 \quad \text{in } \Omega, \quad (1)$$

$$(\lambda \operatorname{tr}(\epsilon(\mathbf{U})) \mathbf{I} + 2\mu \epsilon(\mathbf{U})) \cdot \mathbf{n} = \mathbf{g} \quad \text{on } \Gamma_N \cup \Gamma_H, \quad (2)$$

$$\mathbf{U} = \mathbf{W} \quad \text{on } \Gamma_D, \quad (3)$$

where λ and μ are the Lamé constants, $\epsilon(\mathbf{U}) = \frac{1}{2}(\nabla \mathbf{U} + (\nabla \mathbf{U})^T)$ the infinitesimal strain tensor, $\mathbf{g} \in L^2(\Gamma_N \cup \Gamma_H)$ the applied traction and $\mathbf{W} \in H^1(\Omega)$ the imposed displacements. The body forces are neglected. Due to the symmetries shown in Figure 1, only the upper right quarter is modelled. Only the plane strain problem is treated in Alberty et al. (2002) so that the Lamé coefficients are related to the Young's modulus E and the Poisson's ratio ν through $\lambda = E\nu/((1+\nu)(1-2\nu))$ and $\mu = E/(2(1+\nu))$. The introduction of a fictitious Young's modulus $E^* = E(1+2\nu)/(1+\nu)^2$ and Poisson's ratio $\nu^* = \nu/(1+\nu)$ readily transforms the plane strain assumption into a plane stress one without requiring any modification of the given program. The corresponding weak form of the elasticity problem stated above is:

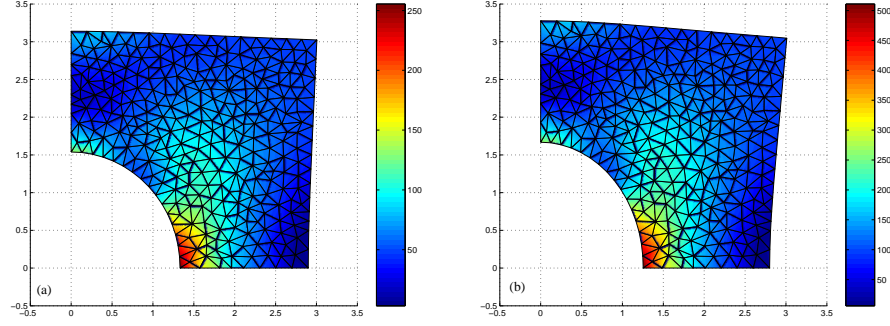


Figure 2: **(a)** and **(b)**: Map of the von-Mises stresses for the surface load $\mathbf{g} = 50\mathbf{j}$ and $\mathbf{g} = 100\mathbf{j}$ respectively on the upper boundary.

Find $\mathbf{U} \in H^1(\Omega)$ such that for all $\mathbf{V} \in H_D^1(\Omega) := \{\mathbf{V} \in H^1(\Omega) : \mathbf{V} = 0 \text{ on } \Gamma_D\}$,

$$\int_{\Omega} \epsilon(\mathbf{V}) : \mathcal{C}\epsilon(\mathbf{U}) dx = \int_{\Gamma_N \cup \Gamma_H} \mathbf{g} \cdot \mathbf{V} ds, \quad (4)$$

where the elasticity tensor \mathcal{C} is given by,

$$\mathcal{C} = \begin{pmatrix} \lambda + 2\mu & \lambda & 0 \\ \lambda & \lambda + 2\mu & 0 \\ 0 & 0 & \mu \end{pmatrix}. \quad (5)$$

Equation (4) is discretised using the standard Galerkin method and linear triangular elements. Each iteration of the fixed point iterative scheme described in the following section produces a new contour of the hole, and re-meshing is necessary. The freely available mesh generator Triangle is used to this end (Shewchuk (2002)). In order to ensure the quality of the mesh, constraints of 30° on the minimum admissible angle and of 0.02 on the maximum admissible triangle area are imposed.

Figure 2 illustrates the deformation of the membrane when the hole is a circle of radius $\sqrt{2}$, $L_0=3$, $E=2900$ Pa and $\nu=0.4$. The membrane is stretched vertically so that $\mathbf{g} = \beta\mathbf{j}$ on the upper boundary (\mathbf{j} is the vertical unit vector) and the rest of the boundary is traction free. To impose symmetry boundary conditions, the horizontal displacements are imposed to vanish on $\{0\} \times [\sqrt{2}, 3]$ and the vertical ones on $[\sqrt{2}, 3] \times \{0\}$. Figure 2 also shows the von-Mises stress σ_{VM} computed as follows

$$\sigma_{VM} = \sqrt{\sigma_1^2 + \sigma_2^2 - \sigma_1\sigma_2} \quad (6)$$

where σ_1 and σ_2 are the principal stresses equal to

$$\sigma_{1,2} = \frac{\sigma_{xx} + \sigma_{yy}}{2} \pm \sqrt{\left(\frac{\sigma_{xx} - \sigma_{yy}}{2}\right)^2 + \sigma_{xy}^2}. \quad (7)$$

A feature worth mentioning is the "linearity" of the membrane's response. As the load is doubled from 50 Pa to 100 Pa, the maximum value of the maximum von Mises stress also doubles from ~ 250 to ~ 500 . One would expect that the difficulty of the identification of the required initial contour becomes greater as the value of the load increases since the deformed geometry defers more and more from the initial one.

3 Description of the Fixed Point Iterative Schemes

In order to describe the algorithm which tackles the inverse problem of identifying the required initial shape, the notations are first detailed. A number of points are introduced on the contour Γ_H of the perforated hole. These points naturally correspond to the boundary nodes of the mesh. Let M_1^d, \dots, M_L^d denote the L boundary nodes of the desired contour of the hole after deformation, and $M_1^{ini}, \dots, M_L^{ini}$ denote the associated L boundary nodes of the required initial contour (solution to the inverse problem). The M_i^{ini} are found iteratively as the limit of a

series of M_i^j , where the superscript j denotes the iteration number. At each iteration, N_i^j corresponds to the new location of the node M_i^j in the deformed configuration, and U_i^j is the associated displacement. The algorithm is best described in pseudo-code notation as follows.

1. First iteration: use M_i^d , $i \in [1, L]$ as a first guess to M_i^{ini} , $i \in [1, L]$ and calculate the *residual vector* Δ_i^1 , $i \in [1, L]$ the norm of which gives a measure of how far the node in the deformed geometry is located from the desired location:
for i=1 to L {

$$\mathbf{OM}_i^1 = \mathbf{OM}_i^d; \quad (8)$$

$$\mathbf{ON}_i^1 = \mathbf{OM}_i^1 + \mathbf{U}_i^1; \quad (9)$$

$$\Delta_i^1 = \mathbf{OM}_i^d - \mathbf{ON}_i^1; \quad (10)$$

} j=2;

2. The following iterations: update the previous estimate to M_i^{ini} , $i \in [1, L]$ and calculate the residual vector Δ_i^j , $i \in [1, L]$:

Do {
for i=1 to L {

$$\mathbf{OM}_i^j = \mathbf{OM}_i^{j-1} + \Delta_i^{j-1} + \mathbf{B}_i^j; \quad (11)$$

$$\mathbf{ON}_i^j = \mathbf{OM}_i^j + \mathbf{U}_i^j; \quad (12)$$

$$\Delta_i^j = \mathbf{OM}_i^d - \mathbf{ON}_i^j; \quad (13)$$

} j=j+1;}

While $\max(\|\Delta_i^j\|) > \epsilon$

Restated in simple terms, the initial guess for the required initial location of the boundary node is chosen to be the location of the nodes of the desired hole contour. At each iteration the residual vector (Δ_i^j) the norm of which measures how far the deformed shape is located from the desired one is evaluated and added to the previous guess of the required initial boundary node location. \mathbf{B}_i^j is a corrective term which enlarges the range of applicability of the scheme and shall be defined subsequently. If this corrective term vanishes, the intuitive scheme proposed in Sellier (2005) and illustrated on Figure 3 is recovered. Since this scheme is entirely based on geometric consideration, it does not depend on the material behaviour and should therefore be applicable regardless of the constitutive law.

4 Convergence Analysis

In order to assess the convergence properties of the scheme (i.e. will N_i^j , $i \in [1, L]$ converge to M_i^d , $i \in [1, L]$ for increasing j , and if so, how fast?), it is necessary to note that as a consequence of the algorithm,

$$\Delta_i^j = \mathbf{U}_i^{j-1} - \mathbf{U}_i^j - \mathbf{B}_i^j. \quad (14)$$

This result is proven by simple algebraic manipulations as follows.

Eq. (13) gives

$$\Delta_i^j - \Delta_i^{j-1} = \mathbf{OM}_i^d - \mathbf{ON}_i^j - (\mathbf{OM}_i^d - \mathbf{ON}_i^{j-1}).$$

Substitution of eq. (11) into eq. (12) and of eq. (12) into the previous equation yields

$$\Delta_i^j - \Delta_i^{j-1} = \mathbf{OM}_i^{j-2} + \Delta_i^{j-2} + \mathbf{B}_i^{j-1} + \mathbf{U}_i^{j-1} - (\mathbf{OM}_i^{j-1} + \Delta_i^{j-1} + \mathbf{B}_i^j + \mathbf{U}_i^j),$$

but since according to eq. (11), $\mathbf{OM}_i^{j-1} = \mathbf{OM}_i^{j-2} + \Delta_i^{j-2} + \mathbf{B}_i^{j-1}$, eq. (14) is recovered which proves the result.

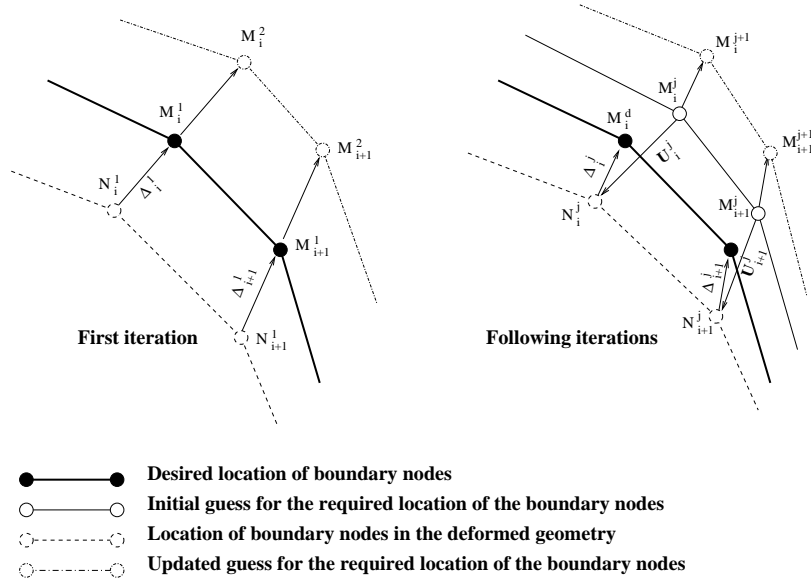


Figure 3: The iterative algorithm with the corrective term \mathbf{B}_i^j set to zero.

At iteration $(j - 1)$, the displacement of the node M_i^{j-1} with coordinates (x_i^{j-1}, y_i^{j-1}) can be found by Taylor series expansion around M_i^d with coordinates (x_i^d, y_i^d) . Accordingly,

$$U_{x_i}^{j-1} = U_x(x_i^d, y_i^d) + \frac{\partial U_x}{\partial x}|_i^d (x_i^{j-1} - x_i^d) + \frac{\partial U_x}{\partial y}|_i^d (y_i^{j-1} - y_i^d) + h.o.t., \quad (15)$$

$$U_{y_i}^{j-1} = U_y(x_i^d, y_i^d) + \frac{\partial U_y}{\partial x}|_i^d (x_i^{j-1} - x_i^d) + \frac{\partial U_y}{\partial y}|_i^d (y_i^{j-1} - y_i^d) + h.o.t., \quad (16)$$

where $(U_{x_i}^{j-1}, U_{y_i}^{j-1})$ are the components of the displacement vector \mathbf{U}_i^{j-1} , and it is understood that the spatial derivatives of the displacement are taken at M_i^d .

Similarly, at iteration (j) , the displacement of the node M_i^j can be written as follows:

$$U_{x_i}^j = U_x(x_i^d, y_i^d) + \frac{\partial U_x}{\partial x}|_i^d (x_i^j - x_i^d) + \frac{\partial U_x}{\partial y}|_i^d (y_i^j - y_i^d) + h.o.t., \quad (17)$$

$$U_{y_i}^j = U_y(x_i^d, y_i^d) + \frac{\partial U_y}{\partial x}|_i^d (x_i^j - x_i^d) + \frac{\partial U_y}{\partial y}|_i^d (y_i^j - y_i^d) + h.o.t.. \quad (18)$$

Subtracting eq. (17) from eq. (15) and eq. (18) from eq. (16) gives,

$$U_{x_i}^{j-1} - U_{x_i}^j = \frac{\partial U_x}{\partial x}|_i^d (x_i^{j-1} - x_i^j) + \frac{\partial U_x}{\partial y}|_i^d (y_i^{j-1} - y_i^j) + h.o.t., \quad (19)$$

$$U_{y_i}^{j-1} - U_{y_i}^j = \frac{\partial U_y}{\partial x}|_i^d (x_i^{j-1} - x_i^j) + \frac{\partial U_y}{\partial y}|_i^d (y_i^{j-1} - y_i^j) + h.o.t.. \quad (20)$$

Moreover, taking eqs. (11) and (14) into account and remembering that $\frac{\partial U_x}{\partial x} = \epsilon_{xx}$ and $\frac{\partial U_y}{\partial y} = \epsilon_{yy}$, these equations may be rewritten as

$$\Delta_{x_i}^j = -\epsilon_{xx}^d (\Delta_{x_i}^{j-1} + B_{x_i}^j) - \frac{\partial U_x}{\partial y}|_i^d (\Delta_{y_i}^{j-1} + B_{y_i}^j) - B_{x_i}^j + h.o.t. \quad (21)$$

$$\Delta_{y_i}^j = -\frac{\partial U_y}{\partial x}|_i^d (\Delta_{x_i}^{j-1} + B_{x_i}^j) - \epsilon_{yy}^d (\Delta_{y_i}^{j-1} + B_{y_i}^j) - B_{y_i}^j + h.o.t. \quad (22)$$

where $(\Delta_{x_i}^j, \Delta_{y_i}^j)$ and $(B_{x_i}^j, B_{y_i}^j)$ are the x-y components of the residual vector Δ_i^j and the corrective term \mathbf{B}_i^j , respectively. If the corrective term vanishes, it is easy to show (see Sellier (2005)) that two extreme cases should produce convergent schemes. The first one corresponds to deformations dominated by volumetric strains (i.e. $\frac{\partial U_x}{\partial y} \ll \epsilon_{xx} < 1$ and $\frac{\partial U_y}{\partial x} \ll \epsilon_{yy} < 1$), while the second is applicable when the deformations are dominated by the

shear terms, i.e. $\epsilon_{xx} \ll \frac{\partial U_x}{\partial y}$ and $\epsilon_{yy} \ll \frac{\partial U_y}{\partial x}$. The scheme without a corrective term will be referred to as **scheme (I)** in the following. A suitable choice for the corrective term \mathbf{B}_i^j should allow for an improved convergence. One immediately sees that if \mathbf{B}_i^j is chosen such that

$$-\epsilon_{xx_i}^d B_{x_i}^j - \frac{\partial U_x}{\partial y} \Big|_i^d (\Delta_{y_i}^{j-1} + B_{y_i}^j) - B_{x_i}^j = 0, \quad (23)$$

$$-\frac{\partial U_y}{\partial x} \Big|_i^d (\Delta_{x_i}^{j-1} + B_{x_i}^j) - \epsilon_{yy_i}^d B_{y_i}^j - B_{y_i}^j = 0, \quad (24)$$

equations (21) and (22) simply reduce to

$$\Delta_{x_i}^j = -\epsilon_{xx_i}^d \Delta_{x_i}^{j-1} \quad \text{and} \quad \Delta_{y_i}^j = -\epsilon_{yy_i}^d \Delta_{y_i}^{j-1}, \quad (25)$$

which clearly defines a convergent scheme providing the absolute value of the strains is smaller than one, which is necessarily the case in small deformations. Note, however, that since the convergence analysis is based on the Taylor expansion of the displacement field around M_i^d and that only the first order terms are retained, its validity is restricted to situations when M_i^j is sufficiently close to M_i^d . Thus, the algorithm only converges when the initial guess is sufficiently close to the solution to the inverse problem. Equations (23) and (24) are rewritten in a more readable form as follows

$$(\epsilon_{xx_i}^d + 1) B_{x_i}^j + \frac{\partial U_x}{\partial y} \Big|_i^d B_{y_i}^j = -\frac{\partial U_x}{\partial y} \Big|_i^d \Delta_{y_i}^{j-1} \quad (26)$$

$$\frac{\partial U_y}{\partial x} \Big|_i^d B_{x_i}^j + (\epsilon_{yy_i}^d + 1) B_{y_i}^j = -\frac{\partial U_y}{\partial x} \Big|_i^d \Delta_{x_i}^{j-1}. \quad (27)$$

Since $\epsilon_{xx_i}^d$, $\epsilon_{yy_i}^d$, $\frac{\partial U_x}{\partial y} \Big|_i^d$ and $\frac{\partial U_y}{\partial x} \Big|_i^d$ must be evaluated at M_i^d , these can be computed in practice at the first iteration, and therefore the system of equations (26) and (27) can be solved at each iteration for the two components of the corrective vector \mathbf{B}_i^j . We denote by **scheme (II)** the one with the corrective term which satisfies equations (26) and (27) exactly.

Finally, a simple analysis of the orders of magnitude reveals that providing $\epsilon_{xx_i}^d \ll 1$, $\epsilon_{yy_i}^d \ll 1$, $\frac{\partial U_x}{\partial y} \Big|_i^d \ll 1$ and $\frac{\partial U_y}{\partial x} \Big|_i^d \ll 1$, the corrective vector reduces to $\mathbf{B}_i^j \simeq \left(-\frac{\partial U_x}{\partial y} \Big|_i^d \Delta_{y_i}^{j-1}, -\frac{\partial U_y}{\partial x} \Big|_i^d \Delta_{x_i}^{j-1} \right)$ and the latter scheme will be referred to as **scheme (III)**.

5 Results

5.1 Artificial Test with a Given Displacement Field

As a test case, a known and prescribed displacement field is considered, and we seek the initial geometry such that the deformed one matches a disc of radius 0.01. The following displacement field is imposed:

$$\mathbf{U} = (U_x, U_y) = (\alpha(x + y), \alpha(x - y)). \quad (28)$$

Of course, in this case an analytical solution to the inverse problem can be found analytically by solving the following system of equations,

$$x_i^d - x_i^{ini} = \alpha (x_i^{ini} + y_i^{ini}) \quad \text{and} \quad y_i^d - y_i^{ini} = \alpha (x_i^{ini} - y_i^{ini}), \quad (29)$$

for (x_i^{ini}, y_i^{ini}) with (x_i^d, y_i^d) belonging to the circle of radius 0.01. This displacement field is, however, a good candidate to assess the proposed method since the terms ϵ_{xx} , ϵ_{yy} , $\frac{\partial U_x}{\partial y}$ and $\frac{\partial U_y}{\partial x}$ will all have the same magnitude equal to α , and this is precisely the situation when, according to the previous analysis, the convergence of **scheme (I)** can not be guaranteed.

The benefit of the proposed scheme becomes clear in Figure 4 (a), (b) and (c). For an increasing value of α , the difference in the convergence behaviour between **scheme (II)** and **schemes (I),(III)** becomes larger. For all values of α , the convergence rate ($\|\Delta_i^j\|/\|\Delta_i^{j-1}\|$) of **scheme (II)** is precisely equal to α in virtue of eqs. (25). It is much worse for **schemes (I),(III)**, and **schemes (I),(III)** even fail to converge for $\alpha = 0.9$. As predicted by the previous

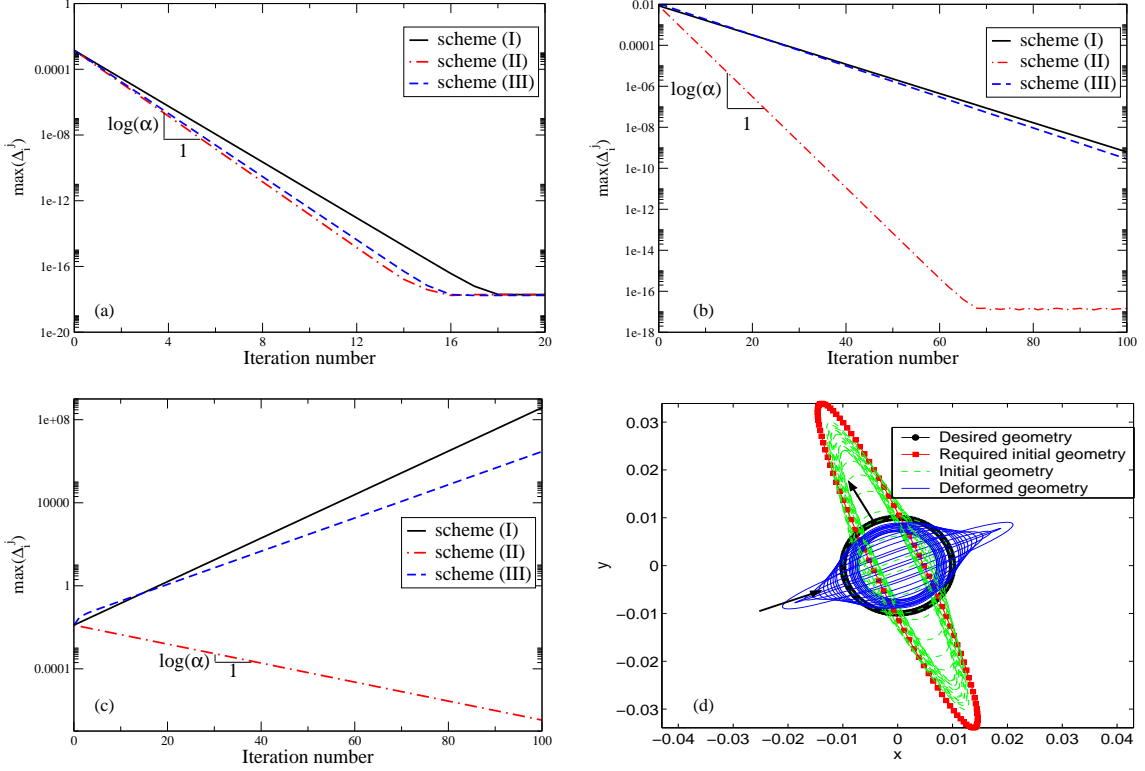


Figure 4: **(a)**, **(b)** and **(c)**: Plot of $\max(\|\Delta_i^j\|)$, $i \in [1, L]$ against the iteration number (j) for $\alpha=0.1, 0.6$ and 0.9 , respectively; **(d)**: Initial and deformed geometries using **scheme (II)**, $\alpha=0.9$ and 100 boundary points ($L = 100$). The arrows indicate the direction of increasing j . The figure also shows the desired geometry and the true required initial geometry (analytical solution).

analysis, the addition of the approximated corrective vector (**scheme (III)**) is only worthwhile for small strains (\sim small α).

5.2 Membrane Hole Design

For the following case, more relevant from an engineering viewpoint, the required initial contour of the perforated hole is sought such that it matches a circle of radius $R_0 = \sqrt{2}$ when the membrane is stretched by the load $\mathbf{g} = \beta \mathbf{j}$. A range of the value of β is considered in order to assess to which extent the schemes are applicable. It can be anticipated that as the value of β rises, the deformation of the hole becomes greater and the difficulty of the inverse problem increases. The material properties and boundary conditions are as described in section 2.

To implement **scheme (II)** and **scheme (III)**, the nodal values of $\epsilon_{xx_i}^d$, $\epsilon_{yy_i}^d$, $\frac{\partial U_x}{\partial y}|_i^d$ and $\frac{\partial U_y}{\partial x}|_i^d$ must be evaluated. Since only piecewise linear elements are used to describe the displacement field, the components of the strain tensor are piecewise constant and the following averaging is used to compute the nodal value of the strains

$$\epsilon_{xx_i}^d = \frac{\sum_{k=1}^{N^e} A_k^e \epsilon_{xx_k}^e}{\sum_{k=1}^{N^e} A_k^e} \quad (30)$$

with analogous expressions for $\epsilon_{yy_i}^d$, $\frac{\partial U_x}{\partial y}|_i^d$ and $\frac{\partial U_y}{\partial x}|_i^d$. A_k^e is the area of one of the N^e elements having the node M_i^d and $\epsilon_{xx_k}^e$ is the corresponding strain. It should be noted that the use of a mixed finite element formulation would improve the estimate of the strains without doubt.

As illustrated in Figure 5 **(a)** and **(b)**, no more than three iterations are necessary to reduce the mismatch between the deformed hole contour and the desired one below the naked eye resolution. Results shown on Figure 5 **(a)** and **(b)** are obtained with **scheme (I)**, 17 boundary nodes ($L = 17$) and $\beta=120$. The scheme is insensitive to the number of boundary nodes, and the number 17 is simply chosen in adequation with the desired mesh density of the domain. Of course, at each iteration care must be taken that no node is introduced by the mesh generator on

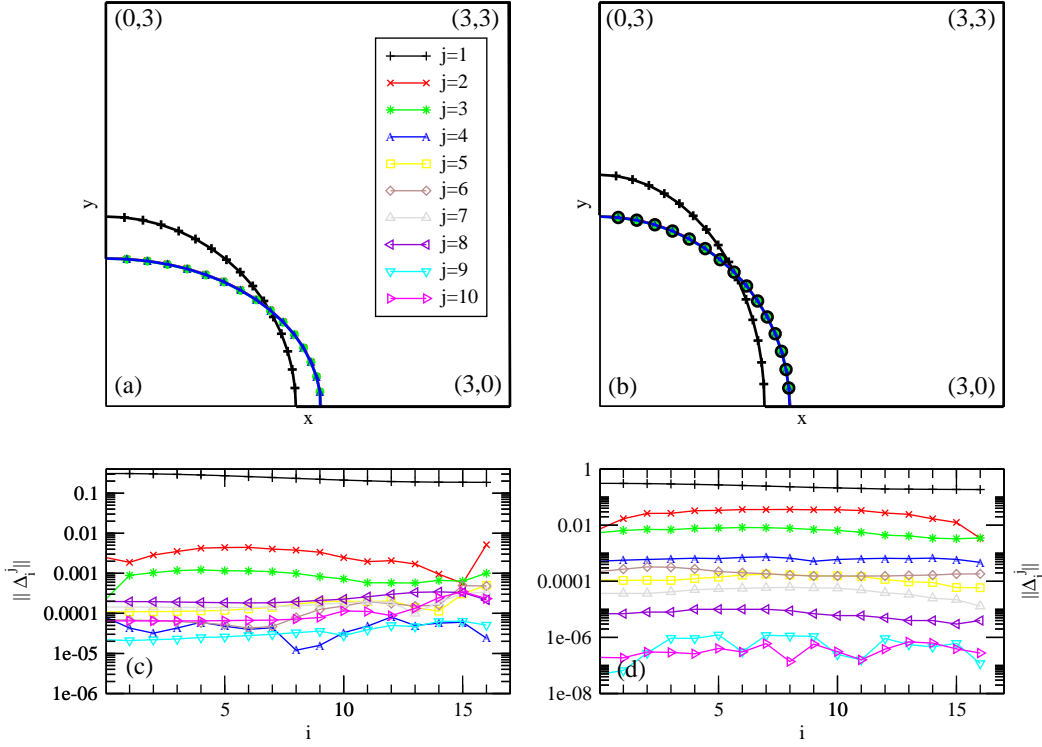


Figure 5: **(a)** and **(b)**: Initial and deformed geometries respectively for $\beta=120$. The circles on Figure **(b)** indicate the targeted hole geometry and **scheme (I)** is employed with 17 boundary points; **(c)** and **(d)**: $\|\Delta_i^j\|$ for $i \in [1, 17]$ and $j \in [1, 10]$ obtained with **scheme (I)** and **scheme (II)** respectively.

Γ_H and that the boundary nodes lie precisely on the location prescribed by eq. (11). Comparing the value of the norm of the residual vector $\|\Delta_i^j\|$ along Γ_H obtained with **scheme (I)** (Figure 5 (c)) and **scheme (II)** (Figure 5 (d)) reveals the significant improvement allowed by the use of **scheme (II)** for this particular value of β . A decrease of more than two orders of magnitude in the mismatch between the deformed and desired shapes is achieved. The **scheme (II)** also appears to yield a more uniform distribution of the norm of the residual vector $\|\Delta_i^j\|$.

A more complete picture is possible by considering Figure 6. The value of β is increased from 10 to 160 by increments of 10 and the mean value of the norm of the residual vector $\|\Delta_i^j\|$ along Γ_H is computed along with the standard deviation according to

$$\text{mean}^j \left(\|\Delta_i^j\| \right) = \frac{\sum_{i=1}^L \|\Delta_i^j\|}{L}$$

$$\text{std}^j \left(\|\Delta_i^j\| \right) = \left(\frac{1}{L-1} \sum_{i=1}^L \left(\|\Delta_i^j\| - \text{mean} \left(\|\Delta_i^j\| \right) \right)^2 \right)^{1/2}.$$

Figure 6 reports the best mean value from a total of 15 fixed point iterations and the corresponding standard deviation for the three schemes. In all tested cases, no improvement of the solution was observed beyond 10 iterations. For β greater than 150, the convergence to the required initial shape worsens for all the schemes and this value can be arbitrarily defined as the upper bound of the applicability range. Below this threshold, the mean value of the residual is reduced by at least 2 orders of magnitude to 2×10^{-4} (at the most) which would be good enough in usual engineering terms. Beyond this threshold, strong oscillations of the solution are observed. Unexpectedly, Figure 6 does not display a monotonous behaviour. As the load decreases, the convergence does not necessarily become easier. For example, the mean distance between the deformed and desired shapes peaks for $\beta=40$ or $\beta=80$. It should be noted, however, that the performance of the three schemes is almost indistinguishable over the load range ($\beta \in [0, 100]$) since the values of the mean distance and standard deviation are almost identical. **Scheme (II)** and **scheme (III)** outperform **scheme (I)** for larger deformations in the range $\beta \in [100, 130]$ confirming the benefit of adding at least an approximated corrective term for the update of the boundary nodes location.

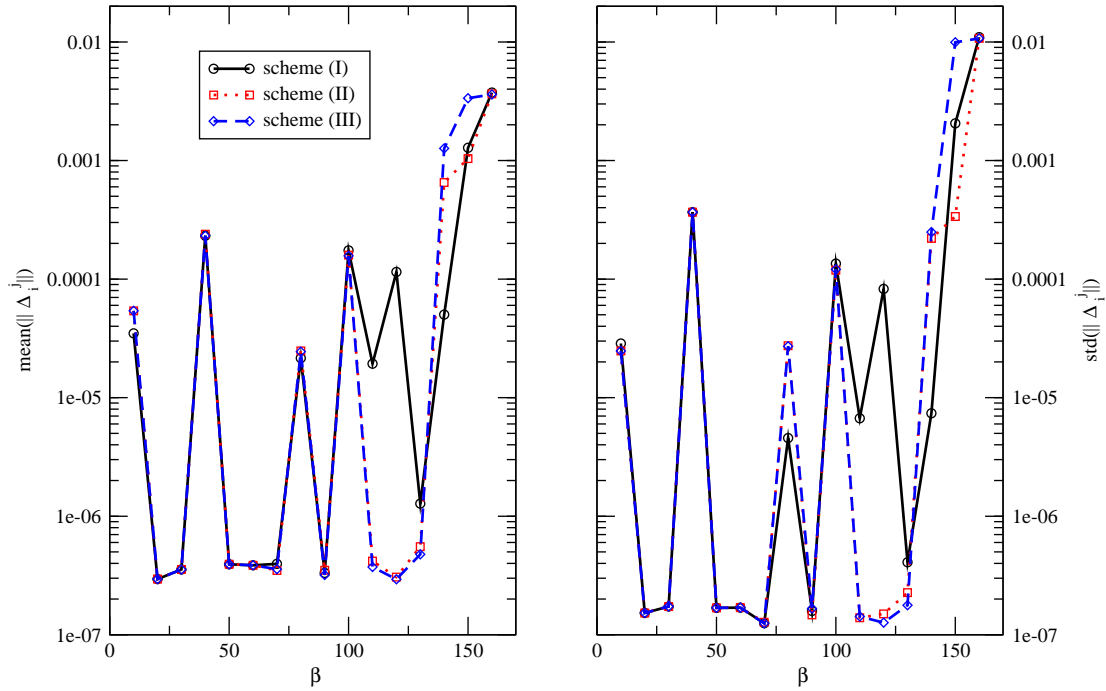


Figure 6: Best mean value from a total of 15 fixed point iterations and the corresponding standard deviation for the three schemes.

6 Conclusions

This paper discusses the possibility of identifying the required initial shape so that the deformed one matches a prescribed shape by means of a fixed point iterative scheme. It consists in using the desired work-piece geometry as an initial guess to the required initial geometry and iteratively updating the locations of a set of boundary points. Based on an analysis of the convergence properties of the scheme, a corrective vector for the update of the boundary point locations is derived. The addition of the latter is shown to extend the applicability of the scheme for the artificial test with a given displacement field and to improve the convergence for the membrane hole design.

This scheme could offer a valuable alternative to other approaches for initial shape identification based on sensitivity analysis and optimization methods. At least four potential benefits may be outlined. No parameterization of the work-piece geometry is required since an arbitrarily large number of boundary points can be selected. The method is purely geometric and therefore its success does not depend on the type of constitutive law. The method can easily be used in combination with a commercial code for the computation of the displacement field. The question of how closely the deformed geometry matches the desired one (which is not necessarily a trivial one) is easily answered thanks to the introduction of the residual vector the norm of which gives a clear measure of the mismatch between the geometries.

Of course, these benefits come at a price which is the lack of robustness of the method as seen on Figure 6 where the best norm of the residual vector unexpectedly peaks (still to an acceptable level) for some values of β . In the view of the ease of implementation of the method, it should nevertheless constitute a first attempt to tackle such inverse problems and prove a valuable engineering technique.

Acknowledgment

The author gratefully acknowledges the funding of the European Union through the MAGICAL project. Special thanks also go to Alberty and co-workers and Shewchuck for kindly making their work on finite element in elasticity and mesh generation freely available.

References

- Alberty, J.; Carstensen, C.; Funken, S.; Klose, R.: Matlab implementation of the finite element method in elasticity. *Computing*, 69, (2002), 239–263.
- Chung, S. H.; Fourment, L.; Chenot, J.-L.; Hwang, S. M.: Adjoint state method for shape sensitivity analysis in non-steady forming applications. *Int. J. Numer. Meth. Engng.*, 57, (2003), 1431–1444.
- Jernberg, A.: A method for modifying tool geometry in order to compensate for springback effects. http://www.dynamore.de/download/eu03/papers/E-III/LS-DYNA_ULM_E-III-45.pdf.
- Park, J. J.; Rebelo, N.; Kobayashi, S.: A new approach to preform design in metal forming with finite element method. *Int. J. Mach. Tool Des. Res.*, 23, (1983), 71–99.
- Pironneau, O.: *Optimal shape design for elliptic systems*. Springer-Verlag, New York (1984).
- Sellier, M.: Optimal process design in high-precision glass forming. *to appear in Int. J. Form. Proc.*.
- Shewchuk, J.: Delaunay refinement algorithms for triangular mesh generation. *Comp. Geom.-Theor. Appl.*, 22, (2002), 21–74.
- Shim, H. B.: Determination of optimal blank shape by the radius vector of boundary nodes. *I. Mech. Eng. B-J. Eng.*, 218, (2004), 1099–1111.
- Shim, H. B.; Son, K. C.: Optimal blank design for the drawings of arbitrary shapes by the sensitivity method. *J. Eng. Mater.-T. ASME*, 123, (2001), 468–475.
- Sokolowski, J.; Zolesio, J. P.: Introduction to shape optimization: shape sensitivity analysis. In: *Springer Series in Computational Mathematics*, Springer, Berlin (1992).
- Son, K.; Shim, H.: Optimal blank shape design using the initial velocity of boundary nodes. *J. Mater. Process. Tech.*, 134, (2003), 92–98.
- Sousa, L. C.; Castro, C. F.; Antonio, C. A. C.; Santos, A. D.: Inverse methods in design of industrial forging processes. *J. Mater. Process. Technol.*, 128, (2002), 266–273.
- Sprekels, J.; Goldberg, H.; Tröltzsch, F.: Numerical treatment of a shape optimization problem in thermoelasticity. citeseer.ist.psu.edu/57118.html.
- Vieilledent, D.; Fourment, L.: Shape optimization of axisymmetric preform tools in forging using a direct differentiation method. *Int. J. Numer. Meth. Engng.*, 52, (2001), 1301–1321.
- Zhao, G.; Wright, E.; V. Grandhi, R.: Forging preform design with shape complexity control in simulating backward deformation. *Int. J. Mach. Tools Manufact.*, 35, (1995), 1225–1239.

Address: Dr. M. Sellier, Fraunhofer-Institut fuer Techno- und Wirtschaftsmathematik (ITWM), Gottlieb-Daimler-St., Geb. 49, 67663 Kaiserslautern, Germany.
email: mathieu.sellier@itwm.fhg.de